The Astrophysical Journal, 685:1262–1269, 2008 October 1

PLASMA FLOWS GUIDED BY STRONG MAGNETIC FIELDS IN THE SOLAR CORONA

Eckart Marsch
Max-Planck-Institut für Sonnensystemforschung, 37191 Katlenburg-Lindau, Germany; marsch@mps.mpg.de

Hui Tian
Max-Planck-Institut für Sonnensystemforschung, 37191 Katlenburg-Lindau, Germany;
Department of Geophysics, Peking University, 100871, Beijing, China

Jian Sun
UCL-Mullard Space Science Laboratory, Holmbury St Mary, Dorking, Surrey, RH5 NT, UK

Werner Curdt
Max-Planck-Institut für Sonnensystemforschung, 37191 Katlenburg-Lindau, Germany

and

Thomas Wiegelmann
Max-Planck-Institut für Sonnensystemforschung, 37191 Katlenburg-Lindau, Germany
Received 2008 March 11; accepted 2008 June 9

ABSTRACT

In this study new results are presented regarding the relationships between the coronal magnetic field and the intensities and Doppler shifts of ultraviolet emission lines. This combination of magnetic field and spectroscopic data is used here to study material flows in association with the coronal field. We introduce the term "coronal circulation" to describe this flow, and to indicate that the plasma is not static but flows everywhere in the extended solar atmosphere. The blueshifts and redshifts often seen in transition region and coronal ultraviolet emission lines are interpreted as corresponding to upflows and downflows of the plasma on open (funnels) and closed (loops) coronal magnetic field lines, which tightly confine and strongly lead the flows in the low-beta plasma. Evidence for these processes exists in the ubiquitous redshifts mostly seen at both legs of loops on all scales, and the sporadic blueshifts occurring in strong funnels. Therefore, there is no static magnetically stratified plasma in the corona, since *panta rhei*, but rather a continuous global plasma circulation, being the natural perpetuation of photospheric convection which ultimately is the driver.

Subject headings: solar wind — Sun: corona — Sun: magnetic fields — Sun: transition region — Sun: UV radiation

1. INTRODUCTION

"Coronal circulation" is a new catchword used here to emphasize that the plasma in the corona is nowhere static but everywhere flowing, strongly guided by the dominant magnetic field. The associated mass is likely supplied to and lost from the corona by various magnetic channels through the boundary set by the inner photosphere/chromosphere interface. Through coronal condensation, mass may be drained into loops (e.g., by diffusive flux-tube filling via collisions) or fall freely on locally open field lines back to the chromospheric interface. Coronal circulation presumably extends to the corona's outer interface, which is assumed to be located near the so-called magnetic source surface (at 2.5–3 $R_\odot$), where the solar wind/heliospheric field actually begins.

The overall quasi-steady solar wind may effectively start only at this surface, and will emanate as the merger of all joined upflows from funnels (perhaps already supersonic; Marsch & Tu 1997) and other open-field regions expanding between the closed loops, which are clearly visible in the *SOHO* images and *TRACE* movies. Most coronal plasma is permanently confined and recycled by circulation, but some fraction can escape as tenuous solar wind, being a mixture of local outflows and "evaporation" from the hottest outer corona, with much smaller plasma content than in lower-lying loops.

In this paper, we provide observational evidence in support of the coronal circulation scenario by a discussion of the relevant existing literature and a presentation of new results regarding the relationships between the coronal magnetic field and the intensities and Doppler shifts of transition region (TR) lines of O IV and Ne VIII, and a coronal line of Fe XII. Since open and closed field lines reach different heights, we trace selected magnetic field lines as they go up and down in the solar atmosphere in order to illustrate basic coronal structures, such as magnetically open (funnels) and closed (loops) lines, and to establish their association with the intensities and red/blueshifts of the O IV, Ne VIII, and Fe XII emission lines. This combination of field and plasma data is then used to study coronal plasma flows associated with the magnetic fields.

Imaging and spectroscopy in far- and extreme-ultraviolet (EUV) light are the standard tools for rendering the plasma visible and analyzing its state by measuring the radiances, widths, and Doppler shifts of the emission lines originating from many heavy ions. (For a recent review of this field, see Wilhelm et al. 2004, 2008.) The space missions *SOHO* (*Solar and Heliospheric Observatory*), *TRACE* (*Transition Region and Coronal Explorer*), and currently *Hinode* have provided unprecedented views of coronal structures, such as streamers, prominences, loops, and active regions (ARs), and unravelled their complex magnetic fields by imaging the plasma confined therein (for a review of this intricate and dynamic corona, see Aschwanden et al. [2001], and for a modern textbook see Aschwanden [2004]).

The solar corona is known to be structured on all scales by the Sun's dominating magnetic field, which controls the transport of mass, energy, and momentum in the corona. The activity and

dynamics of the field are also believed to play a key role in the heating and spatio-temporal evolution of the plasma at all scales. Our current knowledge of the coronal magnetic field largely stems from extrapolations of the measured field in the photosphere and chromosphere, to greater heights. The techniques for computing the force-free magnetic field in the corona are described by Wiegelmann & Neukirch (2002, 2003), and comprehensively discussed in the recent review by Wiegelmann (2008).

2. EXTRAPOLATION OF CORONAL MAGNETIC FIELDS

We obtain the required coronal magnetic field with the help of a linear force-free-field extrapolation code based on the method developed by Seehafer (1978). The code uses a line-of-sight magnetogram, e.g., as observed with *SOHO*/MDI (Michelson Doppler Imager), as input, and has one free parameter. We specify this linear force-free-field parameter α as follows. The three-dimensional coronal magnetic field lines for several different values of α are computed and projected onto two-dimensional coronal ultraviolet images, obtained here from *SOHO*/SUMER (Solar Ultraviolet Measurements of Emitted Radiation) and *Hinode*/EIS (EUV Imaging Spectrometer). The projected magnetic field lines and the coronal EUV loops are compared, assuming that the emitting coronal plasma outlines the magnetic field, and consequently that the emissivity gradient parallel to the field is significantly smaller than in the perpendicular direction. Our method finds the optimum value of α and determines the footpoints of the loops. The details of this method are described in Wiegelmann et al. (2005a). We found an optimal value of $\alpha = 7.4 \times 10^{-9}$ m^{-1} for the SUMER data and $\alpha = 8.1 \times 10^{-9}$ m^{-1} for the EIS data. This force-free parameter α turned out to be close to that in Marsch et al. (2004), and we found that there is a good correspondence between the extrapolated loops and loops seen in the intensity images of the two ARs investigated subsequently.

For the calculation of their magnetic fields, we used two magnetograms which were taken by the MDI close to the observation times of the events studied by the spectrometers. The correction of the magnetogram and the co-alignment of the magnetogram with the SUMER images were carried out by applying the method described in Tu et al. (2005a, 2005b), and are not discussed further here. The co-alignment between EIS and MDI was also carried out by using a cross-correlation technique similar to that in Tu et al. (2005b). We used the force-free-field extrapolation method to construct the coronal magnetic field in a rectangular box, defined by a region which is, with several 100 Mm extension (to avoid boundary effects), much larger in size than the scanning fields of view of SUMER or EIS, and which reaches up to about 280 Mm above the photosphere.

Those field lines reaching the sides and ceiling of the calculation box are defined as open; otherwise they are considered closed. In Figures 1, 2, and 3, we projected the extrapolated magnetic field lines onto the x-y plane, where x is the east-west direction and y is the south-north direction. The size of the extrapolation box is $1024'' \times 524'' \times 270$ Mm for Figure 1, and $900'' \times 700'' \times 285$ Mm for Figures 2 and 3, where the last number in the triple refers to the box height or location of its ceiling in the z-direction. These boxes are certainly large enough to study a typical AR. Since these boxes are much larger than our EIS and SUMER field of view, we only show parts of them in the figures.

The yellow and green lines in the figures indicate closed and open field lines, respectively, in the above sense. More precisely, we may consider a field line to be really open only if it reaches the source surface at 2.5 $R_\odot$, as discussed in the introduction. We cannot show this conclusively with the data set available, so here "open" only means that a field line reaches a height of about or more than 280 Mm, or spans a wider range of horizontal distance, typically about half the size of the box, i.e., about $400''$. Such field lines most likely belong to large and extended coronal loops.

3. SPECTROSCOPIC DATA SETS AND THEIR ANALYSES

Now we present the data analysis of the emission lines Fe XII (19.51 nm), O IV (78.77 nm), and Ne VIII (77.04 nm) as observed in the two ARs. The data were obtained by EIS (Culhane et al. 2007) on *Hinode* and SUMER (Wilhelm et al. 1995; Lemaire et al. 1997) onboard *SOHO*. We here concentrate on the Doppler shifts of these lines. There were no cold chromospheric lines in the spectral windows used by SUMER and EIS, which we could have used for an absolute wavelength calibration. Instead, we assumed a vanishing Doppler shift for each line when averaged over the whole field of view. In this way we calibrated the wavelength and obtained the Doppler velocity maps, which are presented in Figures 1, 2, and 3, together with line intensity maps. Negative values in Doppler shift correspond to blueshifts (toward the observer), and positive ones to redshift (away from the observer).

The EIS data analyzed here pertain to a solar active region (AR) and were obtained from 02:54 to 07:23 on 2006 December 2. More detailed information on this AR and its plasma parameters has previously been given in Doschek et al. (2007). During this period, EIS used a slit ($1'' \times 256''$) with 512 rastering steps to scan the AR NOAA 10926 near the disk center. The EIS pixel size is $1''$, the spectral resolution is 0.00223 nm pixel^{-1}, and the exposure time is 30 s in that data set. The standard EIS procedures for correcting and calibrating the data were applied, including dark-current subtraction, removing of the effects of cosmic rays and hot pixels, and wavelength and absolute calibration.

After these calibrations, each observed line was fitted by a single Gaussian curve, complemented by a constant and a linear term describing the background spectrum. The total counts and line center can be obtained for each spectral profile from this single Gaussian fit. The fitted line center was further corrected by taking into account the slit-tilt effects and the variation of the line position, which is caused by thermal effects on the instrument during the spacecraft orbital motion. Finally, the line-of-sight velocity of an ion can be inferred by using the Doppler-shift formula $v_{\rm los} = c(\lambda - \lambda_0)/\lambda_0$, where λ_0 is the rest wavelength, λ is the actually observed wavelength of any line (the central position of the fitted profile), and c is the speed of light in vacuum. Following these standard procedures, we obtained the intensity and velocity map of Fe XII (19.51 nm) which are shown in Figure 1.

On 2004 May 21, SUMER observed the AR NOAA 0615 from 19:10 to 22:15. The slit 2 ($1'' \times 300''$) was used to scan an area of about $155'' \times 300''$ in this observation. The O IV (78.77 nm) and Ne VIII (77.04 nm) lines were included in the spectral windows. The SUMER procedures for correcting and calibrating the data were applied. They include decompression, flat-field correction, and detector corrections for geometrical distortion, local gain, and dead time. The intensity maps and Dopplergrams of these lines were obtained by applying a single Gaussian fit to each spectrum, and are presented in Figures 2 and 3.

We also estimated the spectral line shift caused by thermal deformations of the optical system of SUMER, as discussed in Dammasch et al. (1999), by averaging the residual line centroid positions across the north-south extension of the slit. In addition, the Doppler shift induced by solar rotation has been taken into account by calculating the line-of-sight velocities for all pixels as a function of their nominal mapping onto the solar disk (Dammasch et al. 1999). We removed these effects before determining the Doppler shifts of spectral lines.

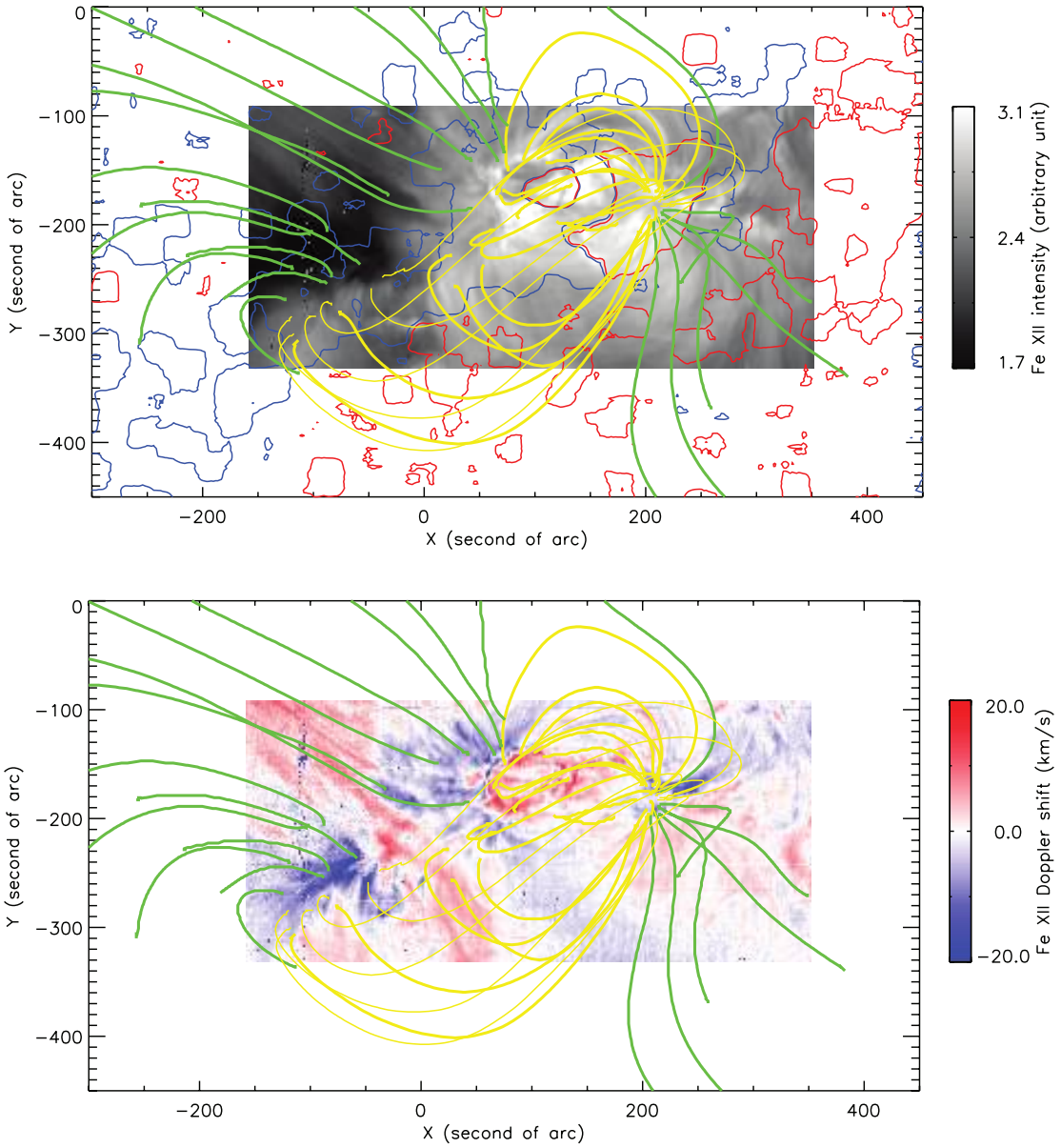

FIG. 1.—*Top*: EIS Fe XII radiance (in arbitrary units) mapped with various magnetic field lines (shown in projection) of the extrapolated coronal magnetic field. The green and yellow lines indicate open and closed field lines, respectively. The intensity is given in the gray scale set by the bar on the right. The spatial solar coordinates are in arcseconds. The red and blue contours indicate the field strength at the 30 G level for opposite polarities. *Bottom*: In similar format, EIS Dopplergram of the corresponding Fe XII line shift. The velocity scale (ranging between −20 and +20 km s^{-1}) is defined by the red/blue bar at the right side. Note that the magnetic field lines start and end in patches of predominantly either red- or blueshift, i.e., footpoints are associated with either up- or downflows.

It is important to note that the loop system shown here in Figures 2 and 3 is identical to the one presented in Dammasch et al. (2008), and although observed 2 days later it still looks very much the same. Similarly, the EIS observed AR NOAA 10926, shown in Figure 1, for nearly 3 days. During this period the data showed no essential change, but indicated that blueshifts on the edge of the AR last for a long time.

4. PLASMA FLOWS IN DIFFERENT CORONAL REGIONS

The data presented in the figures reveal new evidence for both types of flow in the corona, i.e., up- and downflows in different coronal structures, and more importantly, have shown that both red- and blueshifts can last for hours, thus indicating that continuous large-scale plasma flows occur in all types of magnetic structures. We interpret this as strong evidence for quasi-stationary mass circulation in the corona, implying continuous plasma supply to and loss from the corona. We assume that its origin and driver lies in the magnetoconvection below the photosphere in the solar convection zone. Before we discuss our results further, we recapitulate here some relevant previous observations in the more recent literature.

In the last 15 years, a great number of comprehensive ultraviolet imaging and spectroscopic observations have been made with *SOHO* and *TRACE*, and most recently also with *Hinode* (Kosugi et al. 2007). These modern measurements in particular provided ample direct evidence for sizable plasma flows at all heights in the solar corona, with complex multiple-temperature structures, of which the most conspicuous and brightest are the active region (AR) loops (for reviews of this broad subject see, e.g., Kjeldseth-Moe 2003; Brekke 1998; Wilhelm et al. 2008), and the dimmest the coronal funnels (Tu et al. 2005a) in the dark coronal holes (CHs). Hundreds of emission lines in the SUMER

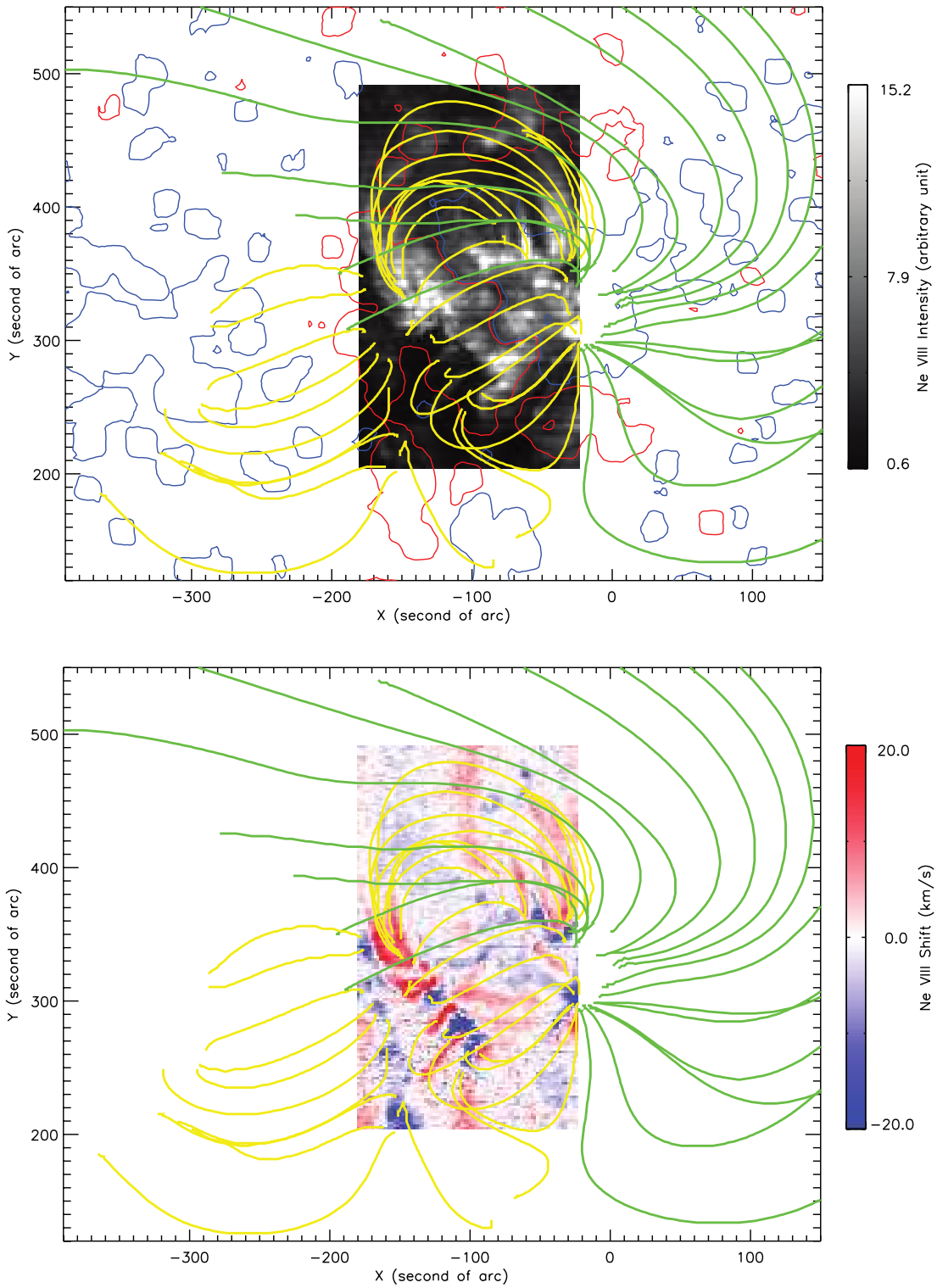

FIG. 2.— *Top*: The SUMER Ne VIII radiance (in arbitrary units) mapped with various magnetic field lines (shown in projection) of the extrapolated coronal magnetic field. The green and yellow lines indicate open and closed field lines, respectively. The intensity is given in the gray scale set by the bar on the right. The spatial solar coordinates are in arcseconds. The red and blue contours indicate the field strength at the 30 G level for opposite polarities. *Bottom*: In similar format, SUMER Dopplergram of the corresponding Ne VIII line shift. The velocity scale (ranging between −20 and +20 km s^{-1}) is defined by the red/blue bar at the right side. Note that the magnetic field lines start and end in patches of predominantly either red- or blueshift, i.e., footpoints are associated with either up- or downflows. In particular, in the area defined by the intervals $x = [-140, -90]$ and $y = [250, 310]$ there are locations with adjacent alternating red/blueshifts and varying magnetic connections to mostly the same Doppler shift at both loop footpoints.

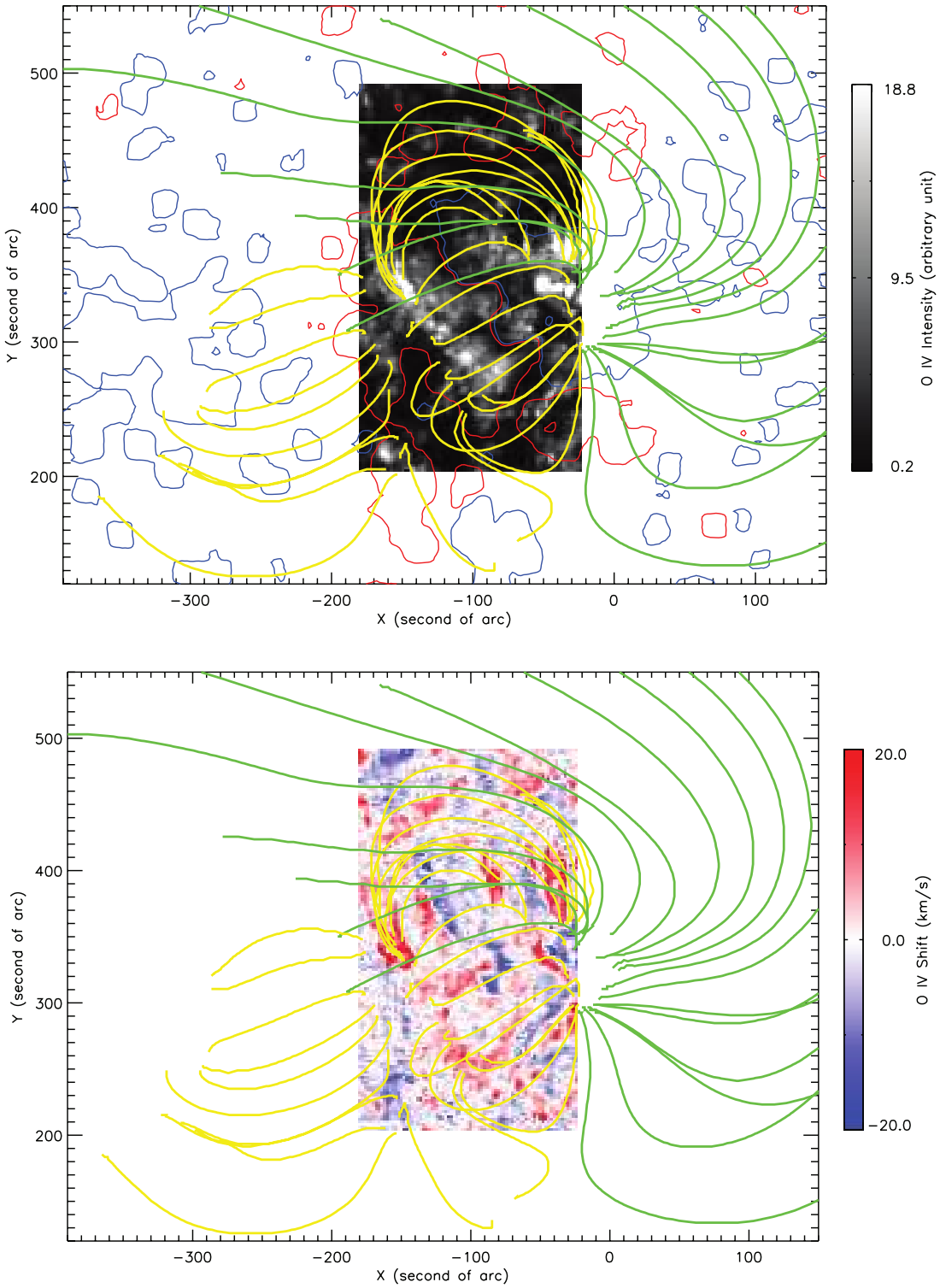

FIG. 3.— *Top*: SUMER O IV radiance (in arbitrary units) mapped with various magnetic field lines (shown in projection) of the extrapolated coronal magnetic field. The green and yellow lines indicate open and closed field lines, respectively. The intensity is given in the gray scale set by the bar on the right. The spatial solar coordinates are in arcseconds. The red and blue contours indicate the field strength at the 30 G level for opposite polarities. *Bottom*: In similar format, SUMER Dopplergram of the corresponding O IV line shift. The velocity scale (ranging between -20 and $+20$ km s^{-1}) is defined by the red/blue bar at the right side. Note that the magnetic field lines start and end in connected patches of predominantly redshift, i.e., both footpoints are associated with downflows. In contrast to Fig. 2, in the area defined by the intervals $x = [-140, -90]$ and $y = [250, 310]$ there are no blue but mostly redshifts at both loop footpoints.

spectral window have been identified and classified in the spectral atlas composed by Curdt et al. (2001, 2004). Many of the bright lines have been used to study coronal structure and TR morphology by means of radiance maps.

Early measurements of TR Doppler shifts were made by the normal-incidence spectrograph flown on *Skylab* (Doschek et al. 1976). Since then, a myriad of studies has accumulated, which are summarized in the recent review of Wilhelm et al. (2008). Here only the Ne VIII (770.428 $\pm$ 0.003 Å) resonance line deserves special mention, because a very accurate value for its rest wavelength was derived by Dammasch et al. (1999). Thus, its shift can well be determined, and this line has often been used as a tracer for plasma bulk flow. It is well known, but not yet understood, that on average the TR the ultraviolet emission lines are redshifted by a few km s^{-1} (Brekke 1993; Chae et al. 1998). This trend also is visible, although not mentioned in that paper, in the data presented in the SUMER spectral atlas (Curdt et al. 2001).

Steady flows in coronal EUV loops were reported by Winebarger et al. (2002) for ARs observed with *TRACE*, and intermittent flows in a bundle of loops above an AR by Winebarger et al. (2001). Previously, Qiu et al. (1999) had already reported counterstreaming mass flows in AR loops, which were visible as apparent motions in the blue/red wings of Hα, and suggested that they were flows associated with filamentary magnetic field strands at the loop footpoints. Possible siphon flows along loops of the AR NOAA 7978B were detected by Spadaro et al. (2000) analyzing SUMER data. Teriaca et al. (1999) also found evidence for motion and upflow in an AR. Patsourakos et al. (2004) investigated whether including a stationary mass flow could explain the discrepancies found between observations and static loop models.

Most recent observations from *Hinode* (Del Zanna 2008; Harra et al. 2008) have clearly shown continuous large-scale patterns of Doppler shifts in TR and coronal lines across ARs. The persistence of the line shifts is unlikely to be accidental; we believe it may signify a global circulation pattern in the corona. From all the above cited papers it seems clear that, for the majority of the loops, redshifts occur in both legs (however, for exceptions see the observations by Tian et al. 2008). As is well known, redshifts are generally larger in cooler lines and tend to occur near the legs of loops. However, according to Del Zanna (2008), it is also obvious that blueshifts are located at AR boundaries and are distinctly higher in the hotter coronal lines. The strongest blueshifts appear in low-density regions, which makes it difficult to observe them and to judge how frequent they really are.

With respect to coronal holes, sizable patches of large blueshift in the Ne VIII line were found in the polar CHs (Wilhelm et al. 2000). Previously, Hassler et al. (1999) had studied in detail the relationship between the Ne VIII Doppler shift and the chromospheric network, using the Si II radiance pattern as a proxy for the network structure, and found that the larger blueshifts in a polar CH were closely associated with the underlying magnetic network and concentrated in its lanes. The links between magnetic field and plasma flow were further studied by Popescu et al. (2004) and Xia et al. (2003) in an equatorial CH, and investigated by Wiegelmann et al. (2005b), who used a simple potential-field extrapolation to represent the magnetic field. These studies were then corroborated by Tu et al. (2005a, 2005b, 2005c), applying the method of force-free-field extrapolation. They found the patches of large Ne VIII blueshift to be connected with open coronal funnels, and in this way identified the magnetic sources of the nascent fast solar wind streams originating in CHs.

In the quiet Sun, large Ne VIII blueshifts were also found in the network lanes, which were also suggested as possible sources of solar wind (Hassler et al. 1999). However, He et al. (2007) reconstructed the coronal magnetic field in the quiet Sun by the method of force-free-field extrapolation and concluded that most of the sites with Ne VIII blueshift were not located in regions of open field, and consequently may not be sources of solar wind. More recently, Tian et al. (2008), using the same method, found strong plasma upflows, again by means of the Ne VIII blueshift as a marker, in coronal loops, and suggested that these flows are not necessarily associated with the solar wind, but may more likely be a signature of mass supply to the loops.

5. DISCUSSION

Some of the papers cited above, and the new results illustrated by our three figures, clearly indicate that continuously occurring motions on all scales seem essential for filling loops and funnels with plasma and emptying them, or maintaining plasma at coronal heights. We recall that such different phenomena as local up and down flows in loop legs, spicules, siphon flows along loops, reconnection jets associated with nanoflares, explosive events, and funnel outflow all are known to cause Doppler shifts of TR and coronal lines. However, as we have found in Figures 1, 2, and 3, the red- and blueshifts seen in large loops and bundles of open fields stay unchanged for many hours, a notion that does not support impulsive events as their origin, but hints more at a steady and lasting systematic process, which we called coronal circulation. However, it may well be the overall integrated net result of many intermittent small-scale events and processes.

By "circulation" we mean here an ongoing and quasi-steady average flow, in either magnetically closed or open structures, and in far-reaching and high-lying coronal loops, as opposed to individual transient flows confined in small and mostly closed magnetic structures. Coronal circulation is not to be confused with these short-lived and small-scale (a few Mm in size) dynamic solar phenomena. We also do not want to compare it with classical convection cells of fluid dynamics, although we do think the inferred permanent flow of coronal material does in some respects resemble mass circulation in a fluid, which is why we think "circulation" describes the observations adequately.

The three figures presented here clearly reveal that the blueshifts are more likely associated with open field lines (e.g., green lines in all the three figures) and with large loops (reaching higher than 100 Mm, e.g., the thin yellow lines in Fig. 1), although there still are some patches of blueshift which correspond to legs of not very high loops (e.g., in the lower left parts of Figs. 2 and 3). It can also be concluded that the redshifts in general are associated with closed field lines. Some elongated features of redshift apparently correspond to the legs of magnetic loops.

Marsch et al. (2004) pointed to the ubiquitous plasma flows in ARs associated with sunspots and to the apparent sharp gradients in the blue/redshift pattern as indicating strong shear flows at the boundaries between open and closed field lines. Recently, Dammasch et al. (2008) also noted that loops with redshifted loop footpoints are very common in the solar atmosphere. The two ARs investigated here confirm that redshifts often are associated with loops, especially their legs. Furthermore, these ARs were scanned by the spectrometers several times, and by a comparison of the different frames (not shown here), we were able to conclude that similar redshifts are associated with the same loops and exist at different times, which implies that they are long-lived and related to steady phenomena.

The prevalence of redshifts observed (Brekke 1993) in ultraviolet lines appears to be a conspicuous property of the solar transition region, apparently indicating ubiquitous downflows. However, the corresponding mass flux would empty large parts

of the corona on timescales of minutes to hours. Overall mass conservation rules out this possibility of mere net downflows. There must be a sufficient steady supply of plasma to the corona to maintain it against solar wind (outer) and chromospheric (inner) losses, i.e., upflows balancing the mass budget are needed. The apparent downflows may likely result from an observational bias due to spatial and/or temporal averaging of the observed plasma motion. Barometric density stratification also causes material to become more easily visible while descending than ascending.

In our Figs. 2 and 3, showing the comparatively cool O IV (formation temperature of 0.16 MK) and hot Ne VIII (0.63 MK) TR lines, in the left frames there are many blueshift patches at the origin of closed (yellow) magnetic field lines of loops, in striking contrast to the Dopplergram of the hot Fe XII (1.3 MK) coronal line in Fig. 3, where blueshift seem to be exclusively connected with open (green) field lines. The blueshifts seen in oxygen and neon emissions may trace bulk plasma flows supplying mass to closed coronal loops, similar to what was found by Tian et al. (2008). On the other hand, in the middle of the Dopplergrams there are also blue patches without any obvious correlation to the morphology of the field lines calculated and drawn here. Since the emission height of these lines seen in projection against the disk is not obvious, it is difficult to establish the links between these blueshift regions and the magnetic field. Since the plasma from which O IV originates is relatively cooler than where Ne VIII mainly is emitted, its location is perhaps lower and thus closer to the denser loop footpoints, and therefore more strongly localized emission and downflows (redshifts) appear in majority.

Therefore, we may miss the outflows required for mass balance in the average coronal observations. As in Marsch et al. (2004), we found in Figure 1 that large patches of the Fe XII blueshift occur near the ARs and are associated with bundles of open magnetic field lines (green color). The abrupt transitions from blueshift to redshift precisely mark the boundaries of open and closed field lines. This blueshift may be a signature of the nascent slow solar wind (Harra et al. 2008) originating from opening loops, or small regions of transiently open fields intermingled with loops. Yet it remains to be shown that these coronal field lines actually continue to large distances, and really become field lines of the inner heliospheric magnetic field.

Dammasch et al. (2008) recently presented SUMER observations revealing steady downflows at transition-region and lower-corona temperatures, as inferred for both footpoints of coronal AR loops associated with sunspots, consistent with our results, particularly in Figure 3. Their findings suggest that the downflows (redshifts) prevailing on all scales in loop footpoints may be a common phenomenon and occur in the entire corona. Significant and lasting adjacent up- and downflows have been detected previously in the sunspot-associated ARs studied by Marsch et al. (2004), who first made use of magnetic field extrapolation for a comparison with and interpretation of the related plasma properties. Recent *Hinode* observations by Sakao et al. (2007) showed that at the edge of an AR, located adjacent to a coronal hole, a pattern of continuous outflow of plasma can be identified, emanating along apparently open magnetic field lines into the higher corona.

These outflows may be indicative of one possible source of the slow solar wind. This is also the conclusion made by Harra et al. (2008), who have provided further observation and evidence of persistent outflows in the iron emission at the edges of an AR as measured by the EIS. The inferred Doppler velocity ranged between 20 and 50 km s^{-1}, consistent with a steady flow seen in the X-ray telescope. Based on an analysis of the AR magnetic field, it was concluded that, when adjusted for line-of-sight effects, the speed could reach over 100 km s^{-1}. This outflow was interpreted as revealing the expansion of loops lying over the AR, which may either reconnect with neighboring large-scale loops or (more likely) open to the upper corona and provide material to the slow solar wind.

6. SUMMARY AND CONCLUSION

By combining coronal observations made by ultraviolet imagers and spectrometers with the coronal magnetic field, we have studied the plasma flows and field structures in different solar regions. We analyzed the connections between ultraviolet radiance and Doppler shift and the topology of the background magnetic field obtained from force-free extrapolation.

We may summarize our results as follows. The plasma flow pattern in the corona is highly structured, and sharp spatial gradients (down to arcsecond scales) were observed, indicating the existence of sizable shear flows. The flow pattern varies with height, but appears to be long-lasting on large scales, thus indicating quasi-steady flows in the entire corona. This steadiness of the global flow pattern may therefore signify systematic, large-scale plasma circulation in the corona. Usually, the interpretation of spectroscopic observations is hampered by the lack of knowledge of the magnetic field and suffers from projection effects of the emission when seen without altitude reference against the solar disk. Our present study partly overcomes this difficulty and emphasizes the need for, and stresses the virtue of, simultaneous measurement and analysis of the magnetic field and plasma. Only through such a combined effort can future studies expect to make further progress in understanding the dynamics and energetics of the active and quiet solar corona.

The SUMER project is financially supported by DLR, CNES, NASA, and the ESA PRODEX Programme (Swiss contribution). SUMER is part of *SOHO*, the *Solar and Heliospheric Observatory*, of ESA and NASA. *Hinode* is a Japanese mission developed and launched by ISAS/JAXA, with NAOJ as domestic partner and NASA and STFC (UK) as international partners. It is operated by these agencies in cooperation with ESA and NSC (Norway). The work of H. T.'s team at PKU is supported by the National Natural Science Foundation of China under contracts 40574078, 40336053, and 40436015. He is now supported by China Scholarship Council for his stay in Germany. The work of T. W. was supported by DLR grant 50 OC 0501.

REFERENCES

Aschwanden, M. J. 2004, Physics of the Solar Corona (Berlin: Springer)
Aschwanden, M. J., Poland, A. I., & Rabin, D. M. 2001, ARA&A, 39, 175
Brekke, P. 1993, ApJ, 408, 735
———. 1998, in ASP Conf. Ser. 155, Second Advances in Solar Physics Euroconference, ed. C. E. Alissandrakis & B. Schmieder (San Francisco: ASP), 150
Chae, J., Yun, H. S., & Poland, A. I. 1998, ApJS, 114, 151
Culhane, J. L., et al. 2007, Sol. Phys., 243, 19
Curdt, W., Brekke, P., Feldman, U., Wilhelm, K., Dwivedi, B. N., Schühle, U., & Lemaire, P. 2001, A&A, 375, 591
Curdt, W., Landi, E., & Feldman, U. 2004, A&A, 427, 1045
Dammasch, I. E., Curdt, W., Dwivedi, B. N., & Parenti, S. 2008, Ann. Geophys., in press
Dammasch, I. E., Wilhelm, K., Curdt, W., & Hassler, D. M. 1999, A&A, 346, 285
Del Zanna, G. 2008, A&A, 481, L49
Doschek, G. A., Bohlin, J. D., & Feldman, U. 1976, ApJ, 205, L177
Doschek, D. G., Mariska, J. T., Warren, H. P., Brown, C. M., Culhane, J. L., Harra, H., Watanabe, T., Young, P. R., & Mason, H. E. 2007, ApJ, 667, L109

Harra, L. K., Sakao, T., Mandrini, C. H., Hara, H., Imada, S., Young, P. R., van DrielGesztelyi, L., & Baker, D. 2008, ApJ, 676, L147
Hassler, D. M., Dammasch, I. E., Lemaire, P., Brekke, P., Curdt, W., Mason, H. E., Vial, J. C., & Wilhelm, K. 1999, Science, 283, 810
He, J.-S., Tu, C.-Y., & Marsch, E. 2007, A&A, 468, 307
Kjeldseth-Moe, O. 2003, in Dynamic Sun, ed. B. N. Dwivedi (Cambridge: Cambridge Univ. Press), 196
Kosugi, T., et al. 2007, Sol. Phys., 243, 3
Lemaire, P., et al. 1997, Sol. Phys., 170, 105
Marsch, E., & Tu, C.-Y. 1997, Sol. Phys., 176, 87
Marsch, E., Wiegelmann, T., & Xia, L.-D. 2004, A&A, 428, 629
Patsourakos, S., Klimchuk, J. A., & MacNeice, P. J. 2004, ApJ, 603, 322
Popescu, M. D., Doyle, J. G., & Xia, L.-D. 2004, A&A, 421, 339
Qiu, J., Wang, H., Chae, J., & Goode, P. R. 1999, Sol. Phys., 190, 153
Sakao, T., et al. 2007, Science, 318, 1585
Seehafer, N. 1978, Sol. Phys., 58, 215
Spadaro, D., et al. 2000, A&A, 359, 716
Teriaca, L., Banerjee, D., & Doyle, J. G. 1999, A&A, 349, 636
Tian, H., Tu, C.-Y., Marsch, E., He, J.-S., & Zhou, G.-Q. 2008, A&A, 478, 915
Tu, C.-Y., Zhou, C., Marsch, E., Xia, L.-D., Zhao, L., Wang, J.-X., & Wilhelm, K. 2005a, Science, 308, 519
Tu, C.-Y., Zhou, C., Marsch, E., Wilhelm, K., Zhao, L., Xia, L.-D., & Wang, J.-X. 2005b, ApJ, 624, L133
Tu, C.-Y., Zhou, C., Marsch, E., Wilhelm, K., Xia, L.-D., Zhao, L., & Wang, J.-X. 2005c, Proc. SW 11-SOHO 16, Connecting Sun and Heliosphere (ESA SP-592; Garching: ESA)
Wiegelmann, T. 2008, J. Geophys. Res. Space Phys., 113, A12, A03S02, DOI: 10.1029/2007JA012432
Wiegelmann, T., Inhester, B., Lagg, A., & Solanki, S. K. 2005a, Sol. Phys., 228, 67
Wiegelmann, T., & Neukirch, T. 2002, Sol. Phys., 208, 233
———. 2003, Nonlinear Processes Geophys., 10, 313
Wiegelmann, T., Xia, L. D., & Marsch, E. 2005b, A&A, 432, L1, DOI: 10.1051/0004-6361:200500029
Wilhelm, K., Dammasch, I. E., Marsch, E., & Hassler, D. M. 2000, A&A, 353, 749
Wilhelm, K., Dwivedi, B. N., Marsch, E., & Feldman, U. 2004, Space. Sci. Rev., 111, 415
Wilhelm, K., Marsch, E., Dwivedi, B. N., & Feldman, U. 2008, Space. Sci. Rev., in press
Wilhelm, K., et al. 1995, Sol. Phys., 162, 189
Winebarger, A. R., DeLuca, E. E., & Golub, L. 2001, ApJ, 553, L81
Winebarger, A. R., Warren, H., van Ballegooijen, A., DeLuca, E. E., & Golub, L. 2002, ApJ, 567, L89
Xia, L.-D., Marsch, E., & Curdt, W. 2003, A&A, 399, L5